Journal of Materials Chemistry C

RSC Publishing

COMMUNICATION

View Article Online
View Journal | View Issue

Fluorine substituted thiophene–quinoxaline copolymer to reduce the HOMO level and increase the dielectric constant for high open-circuit voltage organic solar cells†

Cite this: *J. Mater. Chem. C*, 2013, **1**, 630

Received 3rd October 2012
Accepted 2nd December 2012

DOI: 10.1039/c2tc00327a

www.rsc.org/MaterialsC

Yunzhang Lu,[ab] Zhengguo Xiao,[a] Yongbo Yuan,[a] Haimei Wu,[c] Zhongwei An,[c] Yanbing Hou,*[b] Chao Gao*[c] and Jinsong Huang*[a]

This study reported a novel fluorinated copolymer (FTQ) and shown it to exhibit a significantly higher open circuit voltage (V_{OC}) in bulk heterojunction solar cells with [6,6]-phenyl-C71-butyric acid methyl ester ($PC_{71}BM$) compared to the low band-gap polymer Thiophene–Quinoxaline (TQ). Fluorination lowers the polymer HOMO level effectively which pushes down the highest occupied molecular orbital (HOMO) level of the TQ from −5.36 eV to −5.51 eV and increases the relative dielectric constant from 4.2 to 5.5, resulting in a high V_{OC}. The highest V_{OC} of 950 mV was achieved in the FTQ/PCBM solar cell device. For these optimized blends, the device made of FTQ:$PC_{71}BM$ with a 1 : 1 weight ratio yielded a high power conversion efficiency of 5.3% after a very short time thermal annealing process. These findings will be of importance for achieving high-performance of polymer solar cells by functional group substitution in low band gap polymers.

Introduction

Bulk heterojunction (BHJ) based polymer solar cells (PSCs), consisting of conjugated polymer donors and soluble fullerene derivative acceptors, are promising sustainable solar energy conversion devices with the unique advantages of flexibility, light weight, large-area and low cost production.[1–10] Despite all of these advantages, the relatively low power conversion efficiency (PCE), which depends on the optical and electrical properties of the polymer and the nano-scale morphology of the blend film,[11,12] remains a limitation to its commercialization.[13–15] The PCE of solar cell devices is the product of open-circuit voltage (V_{OC}), short-circuit current density (J_{SC}), and fill factor (FF) of the device under 1 sun illumination. The J_{SC} is determined by the optical bandgap of the semiconducting layer as well as the external quantum efficiency (EQE). The V_{OC} of BHJ PSCs is generally believed to correlate to the difference between the highest occupied molecular orbital level of the electron donor polymers ($HOMO_{Donor}$) and the lowest unoccupied molecular orbital level of the electron acceptor ($LUMO_{Acceptor}$).[16] Therefore one broadly applied strategy to increase the PCE of BHJ PSCs is to reduce the optical bandgap of donor polymers while maximizing the energy offset of $HOMO_{Donor}$–$LUMO_{Acceptor}$. One relatively less studied method to increase the V_{OC} of PSC is to increase the relative dielectric constant (ε) of the polymer blend, which can change the binding energy of charge transfer excitons (CTEs), a precursor of free electrons and holes, and thus impact the V_{OC}.[17]

Combining donor–acceptor (D–A) units in one conjugated co-polymer is an effective method to reduce the optical bandgap by controlling the intramolecular charge transfer.[10,18] By incorporating a strong electron-donating donor unit and a strong electron-withdrawing acceptor unit in the co-polymer backbones, many low band gap conjugated polymers have been demonstrated with absorption edges larger than 700 nm.[19–21] One successful example is poly[2,3-bis-(3-octyloxyphenyl)quinoxaline-5,8-diyl-*alt*-thiophene-2,5-diyl] (TQ)-based copolymers with a low optical bandgap of 1.7 eV which exhibited promising photovoltaic properties.[22,23] Although significant progress has been made to reduce the optical bandgap, one major hindrance for the efficiency enhancement of these BHJ solar cells is the low V_{OC} which is much less than the optical bandgap of the donor polymers.[4,5,24–27]

Adding electron-withdrawing functional groups is an effective approach to push down the HOMO of the donor polymer without increasing the optical bandgap and thus to increase the V_{OC} of the BHJ solar cells without sacrificing the J_{SC}.[28] In this manuscript, we report the increasing V_{OC} of TQ based co-polymer by fluorine substitution of TQ which combines the reduced HOMO level as well as increased dielectric constant.

Poly[6-fluoro-2,3-bis-(3-octyloxyphenyl)quinoxaline-5,8-diyl-*alt*-thiophene-2,5-diyl] (FTQ) was synthesized with an absorption range of 350–730 nm and a low HOMO of −5.51 eV. As

[a]*Department of Mechanical and Materials Engineering and Nebraska Center for Materials and Nanoscience, University of Nebraska-Lincoln, Lincoln, Nebraska 68588-0656, USA. E-mail: jhuang2@unl.edu*

[b]*Key Laboratory of Luminescence and Optical Information, Ministry of Education, Institute of Optoelectronic Technology, Beijing Jiaotong University, Beijing, 100044, China. E-mail: ybhou@bjtu.edu.cn*

[c]*Xi'an Modern Chemistry Research Institute, 168 of East ZhangBa Road, Xi'an, Shaanxi, 710065, P.R.China. E-mail: chaogao74@gmail.com*

† Electronic supplementary information (ESI) available. See DOI: 10.1039/c2tc00327a

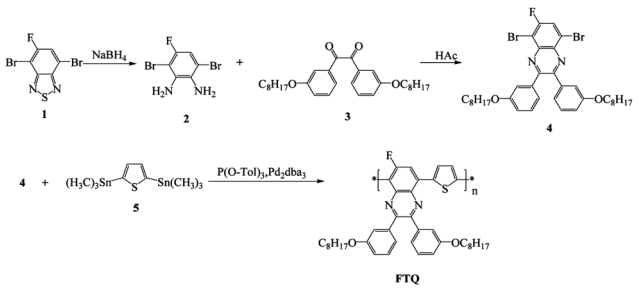

Fig. 1 Synthesis route for FTQ.

shown in Fig. 1, FTQ has a similar structure with the TQ.[23] The fluorine atom has a strong electron withdrawing ability resulting in a 0.1–0.2 eV lower HOMO level than TQ.[28]

Experimental section

Synthetic procedures

4,7-Dibromo-5-fluoro-2,1,3-benzothiadiazole (1) and 2,5-bis(trimethylstannyl)thiophene (5) were purchased from Beijing Allmers Chemical S&T Co., Ltd. 1,2-Bis(3-(octyloxy)phenyl)ethane-1,2-dione (3) was synthesized with the method reported in the literature.[22,23] THF was dried over Na/benzophenone ketyl and freshly distilled prior to use. The synthetic routes of monomers and copolymer are shown in Fig. 1.

3,6-Dibromo-4-fluoro-1,2-phenylenediamine (2)

4,7-Dibromo-5-fluoro-2,1,3-benzothiadiazole (1) (5 g, 0.016 mol) was dissolved in ethanol (150 ml), then sodium borohydride (12.1 g, 0.32 mol) was added portionwise at 0 °C, and the mixture was stirred for 20 hours at room temperature. After evaporation of the solvent, 160 ml water was added and the mixture was extracted with ethyl acetate. The extract was washed with brine and dried over anhydrous magnesium sulfate. The residue was purified by column chromatography on silica gel using hexane–ethyl acetate (25 : 1) as an eluent to afford 3,6-dibromo-4-fluoro-1,2-phenylenediamine (3.5 g) as a pale solid in 78% yield. ^{1}H NMR ($CDCl_3$, 500 MHz) δ (ppm): 6.81(d, 1H, J = 8 Hz), 3.63(br, 4H). ^{13}C NMR ($CDCl_3$, 500 MHz) δ (ppm): 154.16, 152.25, 135.75, 135.73, 128.73, 128.71, 109.44, 109.35, 108.83, 108.62, 96.78, 96.58. Mp: 93–94 °C. Anal. Calcd for ($C_6H_5Br_2FN_2$) (%): C 25.38, H 1.78, N 9.87. Found (%): C 24.29, H 1.83, N 10.14.

5,8-Dibromo-6-fluoro-2,3-bis(3-(octyloxy)phenyl)quinoxaline (4)

A mixture of compound 2 (2.44 g, 8.58 mmol), compound 3 (4 g, 8.58 mmol), and acetic acid (70 ml) was briefly warmed to 60 °C and the solution was then stirred at room temperature for 2 h. The precipitate was collected by filtration, washed with ethanol, and dried to afford 5,8-dibromo-6-fluoro-2,3-bis(3-(octyloxy)phenyl)-quinoxaline 4 (5.83 g) as a white solid in yield 95.23%. ^{1}H NMR ($CDCl_3$, 500 MHz) δ (ppm): 7.94(d, 1H, J = 10 Hz), 7.21–7.24(m, 4H), 7.17(t, 2H, J = 10 Hz), 6.94(m, 2H), 3.86(t, 4H, J = 6.5 Hz), 1.73(m, 4H), 1.29–1.42(m, 20H), 0.89(t, 6H, J = 6.5 Hz). ^{13}C NMR ($CDCl_3$, 500 MHz) δ (ppm): 160.36, 159.09, 158.27, 154.52, 153.29, 139.60, 139.56, 139.00, 138.91, 136.43, 129.36, 122.56, 122.46, 116.72, 115.79, 115.73, 108.21, 108.05, 68.13, 31.56, 29.35, 29.28, 29.12, 26.04, 22.69, 14.12. Mp: 88–89 °C. Anal. Calcd for ($C_{36}H_{43}Br_2FN_2O_2$) (%): C 60.51, H 6.07, N 3.92. Found (%): C 59.96, H 6.14, N 3.97.

Synthesis of FTQ

Compound 4 (375 mg, 0.5 mmol) and 2,5-bis(trimethylstannyl) thiophene (205 mg, 0.5 mmol) were dissolved in a 50 ml dry flask in degassed toluene (15 ml), the mixture was flushed with nitrogen for 30 min, tris(dibenzylideneacetone)dipalladium(0) ($Pd_2(dba)_3$) (9.2 mg) and tri(*o*-tolyl)phosphine (P(*o*-Tol)$_3$) (16.4 mg) were added, then flushed with nitrogen again. Then the mixture was vigorously stirred at 100 °C for 24 h. After cooling down, the solution was poured into methanol. The polymer was collected by filtration and Soxhlet-extracted in order with methanol, hexane, and then with chloroform. The chloroform solution was concentrated to a small volume, and the polymer was precipitated by pouring this solution into methanol. Finally, the polymer was collected by filtration, dried under vacuum at 50 °C overnight and afforded FTQ (244 mg) as a deep-blue solid in yield 73.3%. GPC (tetrahydrofuran, polystyrene standard): M_n = 29.67 kDa, M_w = 68.81 kDa, PDI = 2.33. ^{1}H NMR ($CDCl_3$, 500 MHz) δ (ppm): 7.19–7.33(m, 7H), 6.85(br, 4H), 3.67(br, 4H), 0.68–1.24(m, 33H). Anal. Calcd for ($C_{40}H_{45}FN_2O_2S)_n$ (%): C 75.44, H 7.12, N 4.40. Found (%): C 75.62, H 7.35, N 4.21.

Measurement and characterization of FTQ

^{1}H NMR spectra were recorded on a Bruker Advance 500 spectrometer at 500 MHz, the deuterated $CDCl_3$ was used as a solvent, and the chemical shifts were reported as δ values (ppm) relative to an internal tetramethylsilane (TMS) standard. Molecular weights and distributions of the copolymer were determined using GPC, THF as an eluent and polystyrene as a standard. The absorption spectra were recorded by using a Unico UV-2102 scanning spectrophotometer. The electrochemical cyclic voltammetry was conducted on a CHI 660D Electrochemical Workstation with the Pt disk, Pt wire and Ag/Ag$^+$ electrode as the working electrode, counter electrode, and reference electrode respectively in a 0.1 mol l^{-1} tetrabutylammonium hexafluorophosphate (Bu_4NPF_6) acetonitrile solution. Polymer thin films were formed by drop-casting chloroform solution (analytical reagent, 1 mg ml^{-1}) onto the working electrode, and then dried in air.

Device fabrication and characterization

The structure of the solar cell is Glass/ITO/PEDOT:PSS/Active layer/Ca/Al. As a buffer layer, the conductive polymer PEDOT:PSS (Baytron P VP Al 4083) was spin-coated onto ITO-coated glass substrates, followed by annealing at 130 °C for 20 min to remove water. The thickness of the PEDOT:PSS layer was about 35 nm, as determined by an Ambios Technology XP-2 profilometer. The active layer consisting of FTQ and $PC_{71}BM$ (30 mg ml^{-1} for polymer/PCBM blend) was spin-coated from dichlorobenzene (DCB) solution onto the PEDOT:PSS layer. The active layers were spin-coated in a glove box. All active layers in the fabricated devices were about 100 nm in thickness. Ca (20 nm) and Al (100 nm) were used as top electrodes and deposited *via* a mask in a vacuum onto the active layer. The accurate area of every device defined by the overlap of the ITO and metal electrode was measured carefully by a microscope image.

EQEs were calculated from the photocurrents under short-circuit conditions. PCE was calculated from *J–V* characteristics recorded by a Keithley 2400 Source meter under illumination of an AM1.5G solar simulator with an intensity of 100 mW cm^{-2}. The light intensity was determined by a KG5 filtered silicon photodiode. Device characterization was conducted in an ambient environment. The structure of the contact organic thin-film transistor (OTFT) is Glass/ITO/PVP/FTQ/Ag, which is the same process as solar cell fabrication. The semiconducting films were baked on a hotplate at 110 °C for various minutes to measure different hole mobilities of the film under annealing treatment.

Results and discussion

The FTQ polymer was synthesized with the Stille reaction between 2,5-bis(trimethylstannyl)thiophene and 5,8-dibromo-6-fluoro-2,3-bis(3-(octyloxy)phenyl)quinoxaline with a good yield of 73.3%. The synthesis procedure is shown in Fig. 1 and the synthesis process is described in the Experimental section. Fig. 2a shows the absorption spectra of a FTQ solid thin film and FTQ in $CHCl_3$ solution, respectively. The absorption bands in the film have peaks at 360 nm and 622 nm, and are broader than those in solution where two peaks are found to be 352 nm and 585 nm. The broader absorption spectrum in the solid state indicates an increased π–π stacking form and stronger electronic interaction between the individual polymer chains in the solid state, which is related to its semi-crystalline structure discussed previously.[22] The optical bandgap (E_g^{opt}) deduced from the onset (730 nm) of the polymer absorption spectrum in the films is 1.70 eV, which is close to the ideal bandgap of a donor for BHJ polymer solar cell applications.[29]

The HOMO and LUMO levels of the FTQ polymer were evaluated by cyclic voltammetry (CV) and the results are shown in Fig. 2b. The LUMO and HOMO energy levels of the polymers were estimated from the onsets of oxidation (E_{ox}^{on}) and reduction potential (E_{red}^{on}) values according to the following equation:[30] LUMO $= -e(E_{red}^{on} + 4.72)$ (eV) and HOMO $= -e(E_{ox}^{on} + 4.72)$ (eV), where the potential unit is V *vs.* Ag/Ag^+. So the LUMO and HOMO levels of FTQ can be calculated as −3.08 eV and −5.51 eV, respectively. For comparison, the CV of the synthesized TQ is also included in Fig. 2b. The HOMO of FTQ is 150 meV lower than that of TQ which confirms the function of electron withdrawing fluorine substitution. An energy level diagram of the devices based on TQ and FTQ was constructed as shown in Fig. 2c. It is thus expected that the V_{OC} of the FTQ based BHJ solar cells should be improved by 150 mV compared to TQ. To evaluate this, BHJ PSC devices were fabricated with FTQ and TQ as donors and [6,6]-phenyl-C61-butyric acid methyl ester (PCBM) as an acceptor with a weight ratio of 1 : 3. The photocurrent density–voltage (*J–V*) characteristics of the as-obtained devices are shown in

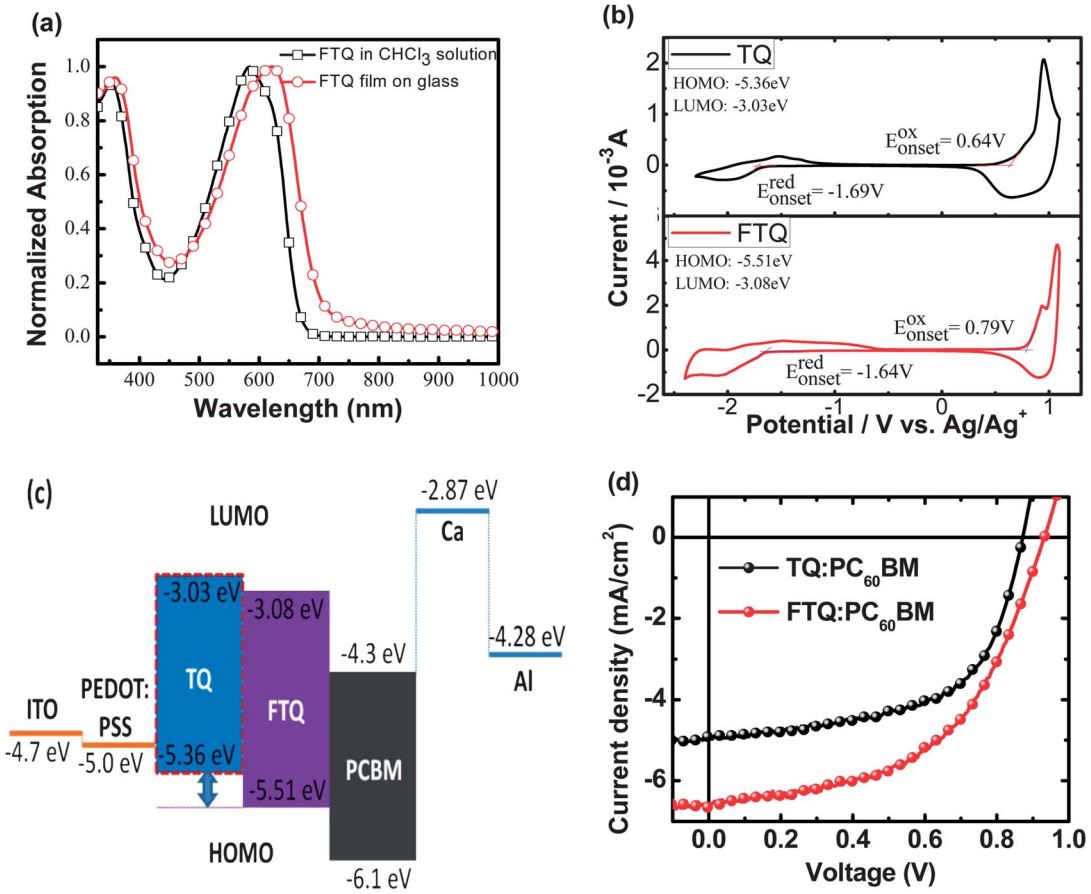

Fig. 2 (a) Normalized absorption spectra of the FTQ in dilute chloroform solution and FTQ solid film. (b) Cyclic voltammograms of TQ and FTQ. (c) Energy level diagram of the component materials and the comparison of the HOMO level of FTQ and TQ. (d) *J–V* curves of TQ:PCBM and FTQ:PCBM devices (1 : 3 w/w), under the illumination of AM1.5G, 100 mW cm^{-2}.

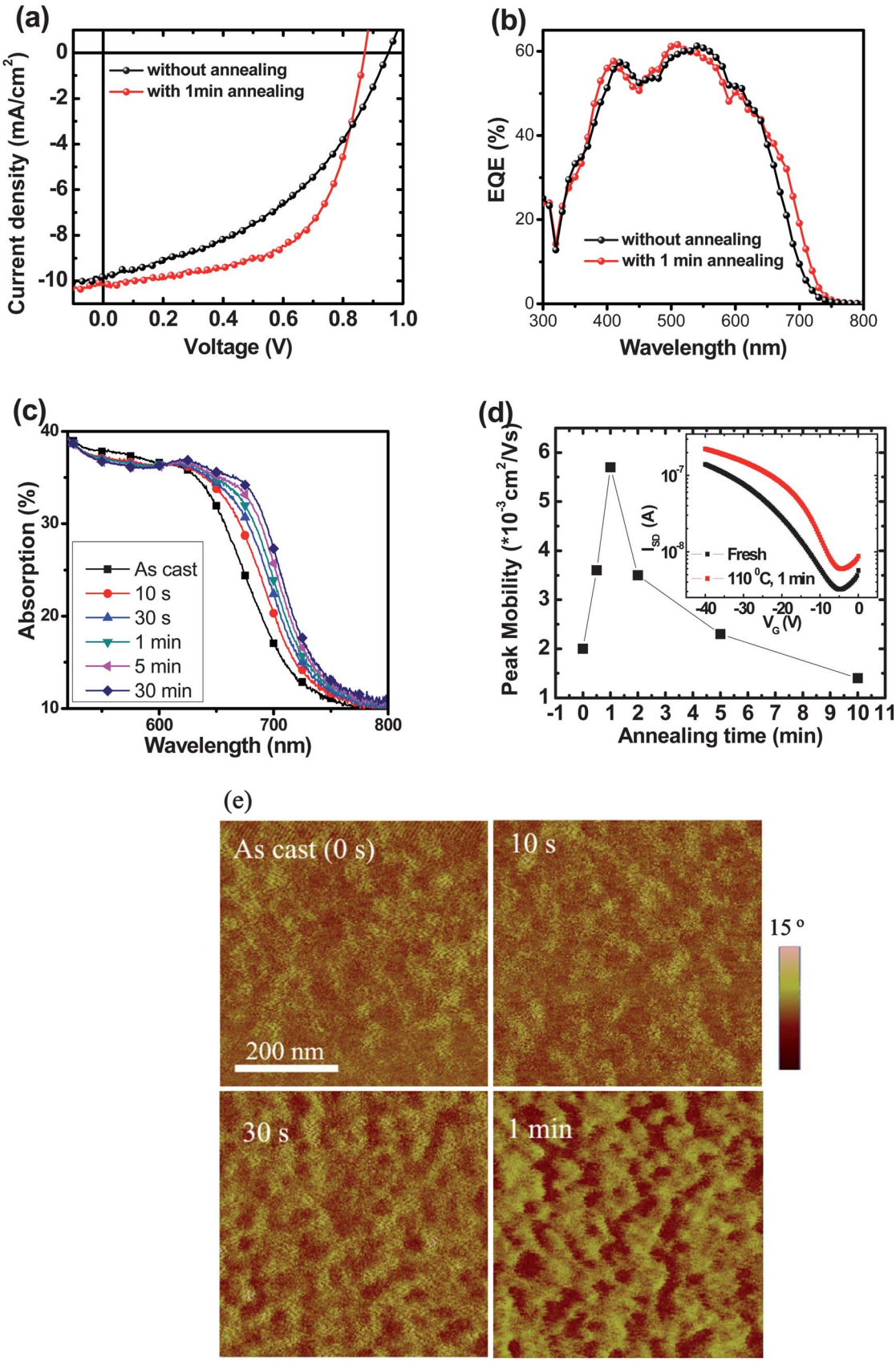

Fig. 3 The effect of thermal annealing treatment on FTQ:$PC_{71}BM$ (1 : 1, w/w) BHJ devices: (a) *J–V* curves, (b) EQE spectra, (c) absorption spectra of a blend film (at 110 °C for different times), (d) FTQ film mobility, and (e) AFM phase images of a blend film (500 nm × 500 nm). For *J–V* curves, both devices were measured under the illumination of AM1.5G, 100 mW cm^{-2}.

Fig. 2d. The TQ based BHJ device has a V_{OC} of 870 mV, comparable to those reported elsewhere.[23] The as-obtained FTQ device exhibited a higher V_{OC} of 932 mV, about 62 mV larger than the TQ based device, which confirms the function of increasing the V_{OC} by fluorine substitution. However, it is noted that the enhancement of V_{OC} is less than that predicted by their relative energy levels, which might be caused by the un-optimized morphology of the active film. The efficiency of the as-obtained FTQ device is 3.21% which is 25% larger than that of the TQ based device.

In order to increase the absorption of the blend around 450 nm, [6,6]-phenyl-C71-butyric acid methyl ester ($PC_{71}BM$) was used as the acceptor to replace $PC_{60}BM$, then a higher J_{SC} of the devices is expected. It is found that the performance of the FTQ based BHJ devices is very sensitive to the short time thermal annealing of the FTQ:$PC_{71}BM$ blend before metal deposition. Fig. 3a shows the *J–V* characteristics of FTQ:$PC_{71}BM$ devices (1 : 1, w/w) with and without thermal annealing. The J_{SC} and especially the FF increased significantly after thermal annealing of the FTQ:$PC_{71}BM$ films at 110 °C for only 1 min. The device with thermally annealed film for 1 min exhibited a J_{SC} of 10.1 mA cm^{-2}, a FF of 60% and a PCE of 5.3%. Fig. 3b shows the corresponding EQE spectra of these devices which are in good agreement with the *J–V* characteristics shown in Fig. 3a. The maximum EQE is well above 60% over a wide spectrum range. Further annealing of the FTQ:$PC_{71}BM$ films over 1 min resulted in deteriorated device performance due to the reduced V_{OC} and FF despite the increased J_{SC}. All the device performance under different thermal annealing conditions is summarized in Table 1. The variation of device performance under thermal annealing can be well-understood by the quick crystallization of FTQ.

The absorption spectra were studied to understand the thermal annealing induced FTQ crystallization at 110 °C for different time scales. Fig. 3c shows the optical absorption spectra of the as-cast FTQ:$PC_{71}BM$ composite films thermally annealed at 110 °C for 10 s, 30 s, 1 min, 5 min and 30 min, respectively. The absorption spectrum of the as-cast FTQ:$PC_{71}BM$ film shows the peak at 620 nm which comes from FTQ. This absorption peak shows a distinct red-shift after thermal annealing for a very short time of 10 s. The red-shift of the absorption peak of polymers is a typical characteristic of the crystallization of conjugated polymers caused by better π–π stacking of the polymer chain.[31] The red-shift of the FTQ absorption spectrum continues with the annealing time and slows down after 30 min thermal annealing. The absorption peak has a redshift of over 50 nm, resulting in a significant increase of FTQ:$PC_{71}BM$ absorption at the wavelength range from 650–750 nm. It is also reflected by the red-shifted external quantum efficiency curves as shown in Fig. 3b. The increased absorption of the FTQ:$PC_{71}BM$ film in the red spectrum band upon thermal annealing explains the increased J_{SC} observed in the device after 1–5 min thermal annealing.

In addition to the broader absorption spectrum, the crystallization of FTQ upon thermal annealing is expected to also increase the hole mobility, which should also contribute to the increase of J_{SC} and FF in the device after 1 min thermal annealing. To find out the influence of thermal annealing on the hole mobility, a bottom-gate, top-contact OTFT device with pure FTQ as the channel layer was fabricated onto a polyvinylpyrrolidone (PVP) dielectric material covered ITO-coated glass substrate. As shown in Fig. 3d, the hole mobility is about 2.0×10^{-3} cm^2 V^{-1} s^{-1} for the pre-heated FTQ film. The hole mobility increases to 5.7×10^{-3} cm^2 V^{-1} s^{-1} after heating at 110 °C for 1 min, which approaches the electron mobility of PCBM (6.0×10^{-3} cm^2 V^{-1} s^{-1}).[32] The more balanced carrier transport in the thermal annealed FTQ:$PC_{71}BM$ film should also contribute to the higher FFs.[13,33] Further annealing of the blend film for more than 1 min leads to a gradual decrease in hole mobility despite even larger crystalline domains being expected, which might be due to the formation of cracks in the FTQ film caused by the crystallization of FTQ at high temperatures.

Although the further thermal annealing at 110 °C for more than 1 min continues to broaden the absorption spectrum, the further increased FTQ crystalline domain size does not necessarily lead to higher PCE of the devices. An extended π–π stacking in larger crystalline domains pulls up the HOMO of FTQ and results in the loss of V_{OC} of the devices with over-annealed FTQ:$PC_{71}BM$ films. In addition, too large size of FTQ domains makes it difficult for the photon generated excitons in FTQ to diffuse to the interface of FTQ and PCBM, which generally causes the severe charge recombination and thus reduced FF.[34] To verify this scenario, the domain size and phase separation of the FTQ:PCBM blend films were measured by tapping-mode atomic-force microscopy (AFM). Fig. 3e shows phase images of FTQ:PCBM (1 : 1, w/w) films under different thermal time treatment conditions. As the annealing time increases, the contrast of the phase becomes clearer which indicates the occurrence of FTQ crystallization. The domain size of the same phase becomes bigger after 1 min thermal annealing. For the blend film without thermal annealing treatment, the surface is smooth with a roughness of 0.32 nm (according to the AFM height images). The roughness increased to 0.44 nm after thermal annealing for 1 min, which indicated the formation of the ordered structure in the FTQ:PCBM thin films.

The composition dependent device performance was studied in conjugation with thermal annealing. The results of *J–V* curves and EQE curves of the devices with various composites before and after thermal annealing are shown in Fig. 4 and their performances are summarized in Table 2. V_{OC} of 910–950 meV was observed for the devices when the polymer:fullerene weight ratio was varied from 1 : 3 to 1 : 0.75 in the BHJ layer shown in Fig. 4a. V_{OC} increases with the FTQ ratio increased in blend and the largest V_{OC} reaches 0.95 V which can be explained by the variation of dielectric constant of the blend films with different PCBM ratios. There has been no conclusion reached yet on how the ratio of PCBM in the polymer:PCBM blend film changes the V_{OC} but it is reasonable to assume that the changed dielectric constant with different donor : acceptor ratios results in a change of V_{OC}. Recent studies

Table 1 Photovoltaic performance of FTQ/$PC_{71}BM$ devices (1 : 1, w/w) with different thermal annealing times at 110 °C, under the illumination of AM1.5G, 100 mW cm^{-2}

Annealing time	J_{SC} (mA cm^{-2})	V_{OC} (V)	FF (%)	PCE (%)
0 s	9.75	0.95	43.3	4.01
10 s	9.88	0.93	45.6	4.19
30 s	9.95	0.89	53.4	4.73
1 min	10.11	0.87	59.9	5.27
5 min	10.23	0.85	55.4	4.82
30 min	6.71	0.81	37.4	2.03

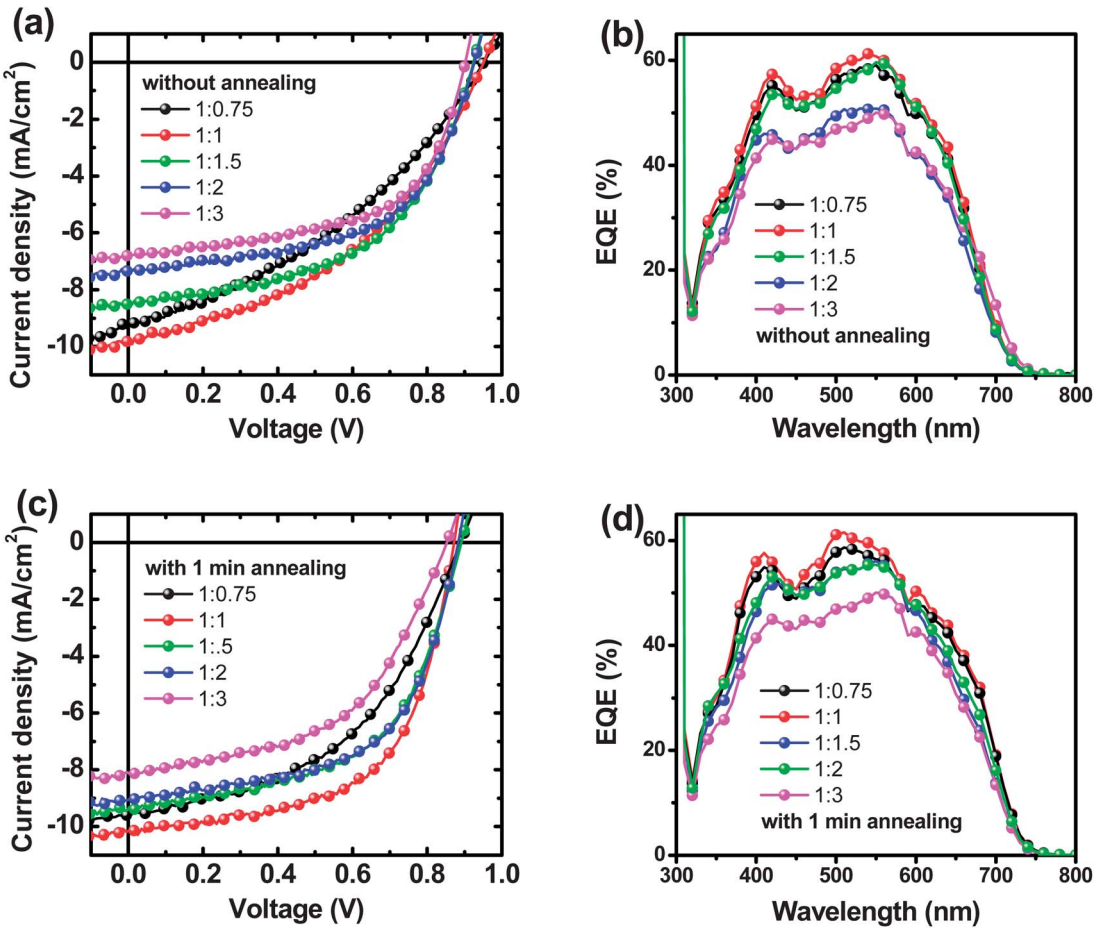

Fig. 4 The effect of the blending ratio on FTQ:$PC_{71}BM$ device performance. (a) and (c) *J–V* curves of the devices with FTQ:$PC_{71}BM$ blending ratios of 1 : 0.75, 1 : 1, 1 : 1.5, 1 : 2 and 1 : 3, under the illumination of AM1.5G, 100 mW cm^{-2}. (b) and (d) EQE spectra for the same devices in (a) and (c), respectively. The devices were treated without (a and b) or with 1 min thermal annealing at 110 °C (c and d).

Table 2 Photovoltaic performance of FTQ/$PC_{71}BM$-based devices (without or with thermal annealing) under the illumination of AM1.5G, 100 mW cm^{-2}

Wt ratio	Annealing conditions	J_{SC} (mA cm^{-2})	V_{OC} (V)	FF (%)	PCE (%)
1 : 0.75	Without	9.13	0.952	37.6	3.27
1 : 1	Without	9.75	0.951	43.3	4.01
1 : 1.5	Without	8.43	0.924	53.3	4.15
1 : 2	Without	7.38	0.927	56.0	3.83
1 : 3	Without	6.81	0.907	57.1	3.52
1 : 0.75	1 min 110 °C	9.61	0.889	47.1	4.03
1 : 1	1 min 110 °C	10.11	0.872	59.9	5.27
1 : 1.5	1 min 110 °C	8.58	0.891	55.9	4.28
1 : 2	1 min 110 °C	7.81	0.883	58.5	4.03
1 : 3	1 min 110 °C	7.29	0.852	50.9	3.16

have shown that there is a linear correlation between the bandgap of CTE (E_g) and the V_{OC} of the solar cells by the following equation:[17,35]

$$E_g = (E_{LUMO}^{Acceptor} - E_{HOMO}^{Donor}) - E_B^{CTE} = V_{OC} - E_B^{CTE} \quad (1)$$

where $E_{LUMO}^{Acceptor}$ is the LUMO of the acceptor, E_{HOMO}^{Donor} is the HOMO of the donor, and E_B^{CTE} is the CTE binding energy. The CTE binding energy is determined by ε of the polymer blend:[36,37]

$$E_B^{CTE} = \frac{q^2}{4\pi\varepsilon_0\varepsilon r} \quad (2)$$

where ε_0 is the vacuum dielectric constant (8.85×10^{-12} F m^{-1}) and r is the radius of the CTE. It is clear that a large dielectric constant of the polymer:PCBM blend helps the CTE dissociation and reduces the energy loss, and thus leads to a larger V_{OC}.

The relative dielectric constants of both FTQ and TQ were measured with a simple device structure of ITO/PEDOT:PSS/polymer/Al, and the frequency dependent relative dielectric constants are shown in Fig. 5.

It is clear that the fluorine substitution of TQ results in a large relative dielectric constant. For example, the ε of FTQ at 10 kHz was measured to be 5.5 which is higher than that of TQ (4.2) and PCBM (3.9).[36] When the ratio of FTQ increases in the blend film, the ε of the blend film increases and the E_B^{CTE} decreases accordingly. For this analysis, the increased V_{OC} in FTQ based BHJ devices over TQ based BHJ devices should also contribute to the increased dielectric constant of donor polymers by fluorine substitution.

J_{SC} and EQE follow a similar trend when the ratio was increased from 1 : 3 to 1 : 1. FTQ has a wider absorption band than PCBM, and thus the increased ratio of FTQ in the blend can efficiently absorb more incident light, resulting in the increased J_{SC} of the

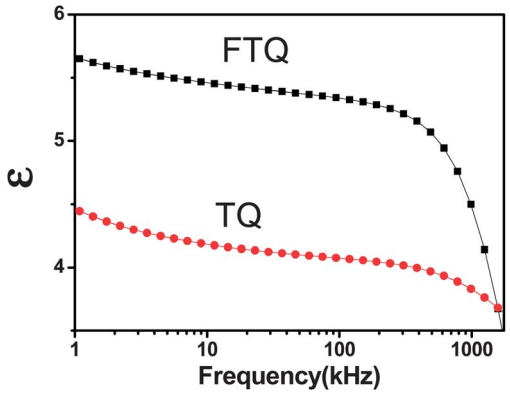

Fig. 5 Variation of relative dielectric constant with frequency using different polymers.

devices. When the FTQ:PCBM ratio was further increased to 1 : 0.75, the J_{SC} and FF of the device decreased. It is expected that too much FTQ in the blend film will result in imbalance of charge transport in the device, which caused lower J_{SC} and FF in the device.[13,33] The devices with the 1 : 1.5 blending ratio exhibit the best performance, with a V_{OC} of 0.924 V, J_{SC} of 8.43 mA cm^{-2} and FF of 53.3%, respectively. Fig. 4b shows the corresponding EQE spectra of these devices which are in good agreement with the *J–V* characteristics shown in Fig. 4a. Fig. 4c and d show the photocurrent and EQE of the devices with the same films but after a short time thermal annealing process (110 °C, 1 min). It is clear that the thermal annealing leads to a larger FF, EQE and J_{SC} for all devices.

Conclusions

In conclusion, fluorine substitution of TQ was shown to effectively push down the HOMO of the TQ, increase the dielectric constant and thus increase the V_{OC} to 950 mV. FTQ possesses an optical bandgap of 1.70 eV, a low-lying HOMO of −5.51 eV, and a good hole mobility up to 5.7 × 10^{-3} cm^2 V^{-1} s^{-1}. The devices made of FTQ:$PC_{71}BM$ with a 1 : 1 weight ratio yielded a high PCE of 5.3% after a very short time thermal annealing process. These findings will be of importance for achieving high-performance of PSCs by functional group substitution in low band gap polymers.

Acknowledgements

J. Huang is grateful for the support from National Science Foundation under Award ECCS-1201384, Y. Lu thanks the State-Sponsored Scholarship for Graduate Students from China Scholarship Council, and C. Gao is grateful for the support from NSFC (Grant no. 60907012, 61177031).

Notes and references

1 R. Søndergaard, M. Hösel, D. Angmo, T. T. Larsen-Olsen and F. C. Krebs, *Mater. Today*, 2012, **15**, 36–49.
2 F. C. Krebs, M. Jørgensen, K. Norrman, O. Hagemann, J. Alstrup, T. D. Nielsen, J. Fyenbo, K. Larsen and J. Kristensen, *Sol. Energy Mater. Sol. Cells*, 2009, **93**, 422–441.
3 S. H. Park, A. Roy, S. Beaupre, S. Cho, N. Coates, J. S. Moon, D. Moses, M. Leclerc, K. Lee and A. J. Heeger, *Nat. Photonics*, 2009, **3**, 297–302.
4 T. Yang, M. Wang, C. Duan, X. Hu, L. Huang, J. Peng, F. Huang and X. Gong, *Energy Environ. Sci.*, 2012, **5**, 8208–8214.
5 Z. He, C. Zhong, X. Huang, W.-Y. Wong, H. Wu, L. Chen, S. Su and Y. Cao, *Adv. Mater.*, 2011, **23**, 4636–4643.
6 Z. He, C. Zhong, S. Su, M. Xu, H. Wu and Y. Cao, *Nat. Photonics*, 2012, **6**, 591–595.
7 C. E. Small, S. Chen, J. Subbiah, C. M. Amb, S.-W. Tsang, T.-H. Lai, J. R. Reynolds and F. So, *Nat. Photonics*, 2011, **6**, 115–120.
8 C. B. Nielsen, R. S. Ashraf, B. C. Schroeder, P. D'Angelo, S. E. Watkins, K. Song, T. D. Anthopoulos and I. McCulloch, *Chem. Commun.*, 2012, **48**, 5832–5834.
9 X. Chen, B. Liu, Y. Zou, L. Xiao, X. Guo, Y. He and Y. Li, *J. Mater. Chem.*, 2012, **22**, 17724–17731.
10 C.-Y. Chang, Y.-J. Cheng, S.-H. Hung, J.-S. Wu, W.-S. Kao, C.-H. Lee and C.-S. Hsu, *Adv. Mater.*, 2012, **24**, 549–553.
11 W. Huynh, J. Dittmer, W. Libby, G. Whiting and A. Alivisatos, *Adv. Funct. Mater.*, 2003, **13**, 73–79.
12 H. Hoppe, M. Niggemann, C. Winder, J. Kraut, R. Hiesgen, A. Hinsch, D. Meissner and N. Sariciftci, *Adv. Funct. Mater.*, 2004, **14**, 1005–1011.
13 G. Li, V. Shrotriya, J. Huang, Y. Yao, T. Moriarty, K. Emery and Y. Yang, *Nat. Mater.*, 2005, **4**, 864–868.
14 W. Ma, C. Yang, X. Gong, K. Lee and A. Heeger, *Adv. Funct. Mater.*, 2005, **15**, 1617–1622.
15 G. Zhao, Y. He and Y. Li, *Adv. Mater.*, 2010, **22**, 4355–4358.
16 C. J. Brabec, A. Cravino, D. Meissner, N. S. Sariciftci, T. Fromherz, M. T. Rispens, L. Sanchez and J. C. Hummelen, *Adv. Funct. Mater.*, 2001, **11**, 374–380.
17 B. Yang, J. Cox, Y. Yuan, F. Guo and J. Huang, *Appl. Phys. Lett.*, 2011, **99**, 133302–133303.
18 J. K. Park, J. Jo, J. H. Seo, J. S. Moon, Y. D. Park, K. Lee, A. J. Heeger and G. C. Bazan, *Adv. Mater.*, 2011, **23**, 2430–2435.
19 A. Ajayaghosh, *Chem. Soc. Rev.*, 2003, **32**, 181–191.
20 C. Yang, S. Cho, R. C. Chiechi, W. Walker, N. E. Coates, D. Moses, A. J. Heeger and F. Wudl, *J. Am. Chem. Soc.*, 2008, **130**, 16524–16526.
21 Y. Hou, G. Long, D. Sui, Y. Cai, X. Wan, A. Yu and Y. Chen, *Chem. Commun.*, 2011, **47**, 10401–10403.
22 T. Yamamoto, B.-L. Lee, H. Kokubo, H. Kishida, K. Hirota, T. Wakabayashi and H. Okamoto, *Macromol. Rapid Commun.*, 2003, **24**, 440–443.
23 E. Wang, L. Hou, Z. Wang, S. Hellström, F. Zhang, O. Inganäs and M. R. Andersson, *Adv. Mater.*, 2010, **22**, 5240–5244.
24 T.-Y. Chu, J. Lu, S. Beaupré, Y. Zhang, J.-R. Pouliot, J. Zhou, A. Najari, M. Leclerc and Y. Tao, *Adv. Funct. Mater.*, 2012, **22**, 2345–2351.
25 Y. Huang, X. Guo, F. Liu, L. Huo, Y. Chen, T. P. Russell, C. C. Han, Y. Li and J. Hou, *Adv. Mater.*, 2012, **24**, 3383–3389.
26 Y. Liang, Z. Xu, J. Xia, S.-T. Tsai, Y. Wu, G. Li, C. Ray and L. Yu, *Adv. Mater.*, 2010, **22**, E135–E138.

27 X. Li, W. C. H. Choy, L. Huo, F. Xie, W. E. I. Sha, B. Ding, X. Guo, Y. Li, J. Hou, J. You and Y. Yang, *Adv. Mater.*, 2012, **24**, 3046–3052.
28 H.-Y. Chen, J. Hou, S. Zhang, Y. Liang, G. Yang, Y. Yang, L. Yu, Y. Wu and G. Li, *Nat. Photonics*, 2009, **3**, 649–653.
29 M. Scharber, D. Mühlbacher, M. Koppe, P. Denk, C. Waldauf, A. Heeger and C. Brabec, *Adv. Mater.*, 2006, **18**, 789–794.
30 J. Hou, Z. a. Tan, Y. Yan, Y. He, C. Yang and Y. Li, *J. Am. Chem. Soc.*, 2006, **128**, 4911–4916.
31 T. J. Savenije, J. E. Kroeze, X. Yang and J. Loos, *Adv. Funct. Mater.*, 2005, **15**, 1260–1266.
32 J. S. Moon, C. J. Takacs, Y. Sun and A. J. Heeger, *Nano Lett.*, 2011, **11**, 1036–1039.
33 S. A. Choulis, Y. Kim, J. Nelson, D. D. C. Bradley, M. Giles, M. Shkunov and I. McCulloch, *Appl. Phys. Lett.*, 2004, **85**, 3890–3892.
34 X. Guo, C. Cui, M. Zhang, L. Huo, Y. Huang, J. Hou and Y. Li, *Energy Environ. Sci.*, 2012, **5**, 7943–7949.
35 K. Vandewal, A. Gadisa, W. Oosterbaan, S. Bertho, F. Banishoeib, I. Van Severen, L. Lutsen, T. Cleij, D. Vanderzande and J. Manca, *Adv. Funct. Mater.*, 2008, **18**, 2064–2070.
36 M. A. Loi, S. Toffanin, M. Muccini, M. Forster, U. Scherf and M. Scharber, *Adv. Funct. Mater.*, 2007, **17**, 2111–2116.
37 T. M. Clarke and J. R. Durrant, *Chem. Rev.*, 2010, **110**, 6736–6767.